

Update of Enhanced Imaging Techniques of Renal Masses Using Apparent Diffusion Coefficient and Diffusion Weighted Magnetic Resonance Imaging

Amal Mohammed ElSayed¹, Inas Mohammed Abd-elaziz ElFiki², Ahmed Mohammed Alaa Eldin³, and Ahmed Fekry Salem⁴

¹MBBCh. Faculty of Medicine-Zagazig University

²Professor of Radiodiagnosis, Faculty of Medicine Zagazig University.

³Assistant Professor of Radiodiagnosis, Faculty of Medicine Zagazig University.

⁴Lecturer of Radiodiagnosis, Faculty of Medicine Zagazig University.

Corresponding author: Amal Mohammed ElSayed

Email: moolygamal27@gmail.com

Abstract

Background: The detection of renal masses has risen significantly over the past years with the increasing use of radiological imaging modalities, majority of renal masses are renal cell carcinoma which account for 80 to 85% of primary renal tumors and approximately 3% of all malignancies in adults. Dynamic contrast-enhanced MRI assesses the signal dynamics caused by contrast material transit through the renal cortex, medulla and the collecting system. Diffusion-weighted imaging (DWI) is a MR modality using strong bipolar gradients to create a sensitivity of the signal to the thermally induced Brownian (or random walk) motion of water molecules and in vivo measurement of molecular diffusion. Magnetic resonance provides a unique opportunity to quantify the diffusional characteristics of a wide range of specimens.

Keywords: Renal masses, Diffusion Weighted Imaging.

1. Introduction:

Renal masses are considered challenge for their proper diagnosis and management that needs interpretation and cooperation between radiologists, clinical pathology specialist, and surgeons.

Classification of renal masses according to The World Health Organization (WHO) published in 2016:(7)

Renal cell tumors

It includes: clear cell renal cell carcinoma, papillary renal cell carcinoma, chromophobe renal cell carcinoma, renal medullary carcinoma, collecting duct carcinoma, multilocular cystic renal neoplasm of low malignant potential, hereditary leiomyomatosis and renal cell carcinoma-associated renal cell carcinoma, mit family translocation renal cell carcinoma, succinate dehydrogenase-deficient renal carcinoma, mucinous tubular and spindle cell carcinoma, tubulocystic renal cell carcinoma, clear cell papillary renal cell carcinoma, renal cell carcinoma, , papillary adenoma and oncocytoma.

Metanephric tumors

It includes metanephric adenoma, metanephric adenofibroma and metanephric stromal tumor. nephroblastic and cystic tumors occurring mainly in children, nephrogenic rests, nephroblastoma, cystic partially differentiated nephroblastoma, and pediatric cystic nephroma.

Mesenchymal tumors occurring mainly in children

Rhabdoid tumor, congenital mesoblastic nephroma, clear cell sarcoma, and ossifying renal tumor of infancy.

Mesenchymal tumors occurring mainly in adults.

Leiomyosarcoma, angiosarcoma, rhabdomyosarcoma, osteosarcoma, synovial sarcoma, ewing sarcoma, angiomyolipoma, epithelioid angiomyolipoma, leiomyoma, hemangioma, lymphangioma, hemangioblastoma, juxtaglomerular cell tumor, renomedullary interstitial cell tumor, and schwannoma, solitary fibrous tumor.

Mixed epithelial and stromal tumor family

Cystic nephroma and Mixed epithelial and stromal tumor.

Neuroendocrine tumors

Well-differentiated neuroendocrine tumor, Large cell neuroendocrine carcinoma, and Small cell neuroendocrine carcinoma.

Miscellaneous tumors

Renal hematopoietic neoplasms and Germ cell tumors of the kidney.

Renal cell carcinomas are the most common malignant renal parenchymal neoplasms. Most renal cell carcinomas grow by expansion and commonly extend into the renal sinus, leading to focal hydronephrosis or caliceal displacement. (1,2).

Unlike transitional cell carcinoma, renal cell carcinoma has a tendency to extend into the venous system. Although indications for partial nephrectomy are constantly changing, the most suitable indication for partial nephrectomy is a renal tumor smaller than 3 cm without invasion of the renal sinus fat, perinephric fat, or renal collecting system, particularly in patients with diminished renal function, a solitary kidney, or bilateral renal malignancy. (1,2).

MR imaging helps delineate the precise location of the renal mass and its relationship to the collecting system and renal vessels. The tumor tends to invade the renal vein and the inferior vena cava with metastases especially to the lung, bone, liver, and brain MR angiography may be an alternative to open biopsy in the evaluation of infiltrating renal neoplasms, the differential diagnosis for which includes urothelial neoplasm, inflammatory lesion, infarct, or infiltrating RCC. Each of these entities, except RCC, is nearly always hypovascular or avascular; therefore, an infiltrating renal mass that is hypervascular strongly suggests an infiltrating RCC (1,2).

2. Renal Masses:**Conventional (Clear cell) renal cell carcinoma**

Clear renal cell carcinomas are the most common subtype of renal cell carcinoma. The average age of onset of sporadic clear cell renal carcinoma is 61 years old. In cases associated with Von Hippel-Lindau disease the average age of onset is 37 years (3).

Clear cell renal cell carcinoma represents around 75-80% of cases of renal cell carcinoma and arises from the epithelium of the proximal tubule. Clear cell carcinoma is sporadic in over 95% of cases, in the 5% of familial cases most are seen in Von Hippel-Lindau disease (3).

Clear cell RCC tends to be hypervascular, with heterogeneous enhancement during the arterial phase. Renal vein tumor thrombus can be seen with aggressive higher-stage tumors. Clear cell carcinomas can also be predominantly cystic with only scant areas of solid enhancing component (2).

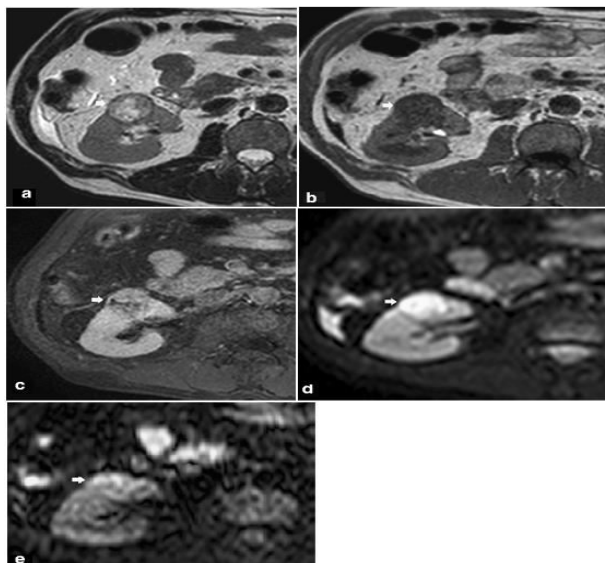


Fig. (1): (a–e) Clear cell renal cell carcinoma in a 65-year-old man. Axial TSE T2W (a) and GE T1W (b) images show hyperintensity and hypointensity of the renal parenchyma mass (arrow), respectively. Axial GE T1W image obtained after gadolinium- based contrast agent administration, during nephrographic phase (c), demonstrates heterogeneous mass enhancement. Axial single-shot echo-planar DWI shows hyperintensity of the mass at $b = 0$ s/mm² (d), remaining hyperintense at $b = 500$ s/mm² (e) indicating restricted diffusion. Quoted from Cova M. et al, (4).

Papillary renal cell carcinoma

Papillary carcinoma (pRCC), characterized by papillary or tubulopapillary histologic architecture, is the second most common subtype of RCC. It may be multifocal in 20–40% of patients. Frequently, it appears on T2W as a low-signal intensity peripheral mass with a low and progressive enhancement. Subtraction images may help in the demonstration of really low-grade enhancement, differentiating pRCC from hemorrhagic cysts (4).

Chromophobe Renal Cell Carcinoma

Chromophobe RCC (cRCC) contains variable proportions of cells with clear or eosinophilic cytoplasm arranged in sheet-like architecture along vascular septae. The prognosis for cRCC is better than in other subtypes of RCC. It typically appears as a well-circumscribed, homogenous renal mass with a cortical epicenter (4).

Medullary Carcinoma

Renal medullary carcinoma is a highly aggressive neoplasm that almost always develops in young patients (11–39 years) with sickle cell trait. In patients with sickle cell trait, there is a chronic hypoxic environment in the renal medulla that eventually leads to transitional cell proliferation involving the terminal collecting ducts and papillary epithelium. The tumor is more prevalent among men younger than 25 years (3:1 male preponderance) in patients over 25 years of age, there is no sex predilection (5).

Collecting Duct Carcinoma

Collecting duct carcinoma is a rare renal tumor that accounts for 1% of all adult malignant renal tumors. It originates from the collecting duct cells. At imaging, the tumors demonstrate a

variegated appearance. They may demonstrate either expansile or infiltrative growth patterns and hypovascular. Calcification is seen in up to 25% of patients. At MRI Collecting duct carcinoma appear as a hypovascular lesion with medullary epicenter, variable signal intensity on T1-weighted images and is frequently hypointense on T2-weighted images. Cystic changes with mural nodules may be seen. Most collecting duct carcinomas are clinically aggressive, with 40% of patients having metastatic disease at presentation (6).

Multilocular cystic renal neoplasm of low malignant potential

MCRN-LMP is a rare cystic tumor of the kidney with an excellent outcome and is composed of multiple cysts separated by thick septa covered with clear cells (7). It was defined as “a tumour composed entirely of numerous cysts, the septa of which contain small groups of clear cells indistinguishable from grade 1 clear cell carcinoma” by Eble et al. (8).

Hereditary leiomyomatosis and renal cell carcinoma-associated renal cell carcinoma

HLRCC syndrome is a recognized distinct phenotypic variant of multiple cutaneous and uterine leiomyomatosis or Reed syndrome, a rare autosomal-dominant condition caused by a mutation in the fumarate hydratase tumor suppressor gene, although patients present with cutaneous leiomyomas, uterine leiomyomas, or both, approximately 33% of these patients will go on to develop renal cell carcinoma typically displaying type II papillary or collecting duct morphology.

Unclassified renal cell carcinoma

Unclassified RCC, as defined by WHO 2016 Classification of the kidney, is a diagnostic category used for renal tumors that do not fit into any of the well-recognized subtypes and includes admixed patterns of more than one recognized subtype: unclassified oncocytic neoplasms or tumors with pure sarcomatoid histology.

Oncocytoma

It is a rare (3% to 6% of renal neoplasms), well-encapsulated, benign tumor composed of eosinophilic cells called oncocytes. Tumors can be large (up to 25 cm), but they average 5 to 8 cm. Hemorrhage and necrosis are rare. Most are solitary, but 6% are multiple or bilateral. Large tumors demonstrate a stellate central scar that is suggestive of the diagnosis. Oncocytes increase in number with age and are found in a variety of organs, including salivary glands, thyroid, pancreas and kidney. In the kidney, oncocytomas arise from the distal tubules or collecting ducts (9).

3. Imaging Techniques of renal masses

Dynamic contrast-enhanced MRI (DCE-MRI) of the kidney

Dynamic contrast-enhanced MRI assesses the signal dynamics caused by contrast material transit through the renal cortex, medulla and the collecting system (10). This technique implies the administration of gadolinium containing contrast agents, which enter the capillaries, are partly filtered in the glomeruli, then pass through the renal tubules or are evacuated by the veins. By analyzing the contrast enhancement as a function of time, several clinically relevant parameters such as blood flow, blood volume, mean transit times and glomerular filtration can be derived. In case of advanced renal insufficiency (GFR < 30 ml/min/1.73m²) the administration of gadolinium containing contrast agents should be avoided, as the risk for nephrogenic systemic fibrosis increases (11).

Technique

Currently no consensus regarding the optimal measurement strategy of renal DCE-MRI exists. The literature shows a large heterogeneity in parameters of pulse sequences, doses of injected contrast media, methods for conversion of signal intensity into concentration and tracer-kinetic analysis. Two fundamentally different approaches must be distinguished:

(i) MR-clearance methods

Use long acquisition times (1–2 h) and slow temporal resolution (20–30 min) to determine GFR from the half-life of the tracer in the body (11).

(ii) MR-renography methods

Use a high temporal resolution and shorter acquisition time (<10 min) to determine GFR and other parameters from the tracer-kinetics inside the kidney itself (12).

Virtually all recent studies used strongly T1-weighted pulse sequences, either in 2D or in 3D mode. 3D acquisition is performed with spoiled gradient-echo (GRE)-sequences, using relatively high flip angles to ensure significant signal changes over a large range of concentrations. Multislice 2D sequences are mostly based on spoiled GRE sequences as well but include a non-selective magnetization preparation pulse (saturation or inversion) and use lower flip angles to reduce the sensitivity to inflow effects. Fast 3D-GRE-sequences, accelerated by parallel imaging and/or keyhole imaging, may allow coverage of the whole organ. DCE-MRI images are commonly acquired in an oblique-coronal plane through the long axis of the kidneys. Compared to transverse planes, fewer coronal planes are required to cover the kidneys and offer the advantage that a large section of the aorta lies in the imaging slab, which helps to reduce inflow effects in the arterial input function (13).

Contrast agents

Low molecular weight gadolinium-chelates have a predominant renal elimination by glomerular filtration without any tubular secretion or reabsorption, and therefore allow for GFR assessment with MRI. The relationship between the DCE-MRI signal changes and the Gd-chelate concentration is not linear at higher concentrations. However, there is a linear relationship between the longitudinal relaxation rate and the Gd-chelate concentration (14).

Because of water re-absorption in the proximal convoluted tubule and within the medulla the concentration of Gd within the kidney may become very high. High concentrations may also be encountered during the first pass in the abdominal aorta and in the renal cortex due to the large blood volumes. Since high concentrations may cause T1-signal saturation and T2*-interference, many studies use less than the regular clinical dose of 0.1 mmol/kg for Gd-chelates, and flow rates are relatively low (14).

Post-processing

A number of strategies exist to minimize or correct breathing motion. Respiratory motion can be minimized by measuring in breath-hold, but multiple sequential breath-holds are required to achieve sufficiently long acquisition times. Alternatively, measurement can be performed using respiratory triggering, but this risks to reduce the temporal resolution below the required level. A combined protocol with breath-hold during the first pass and triggering during the later phases has been proposed as well. As an alternative or complementary to motion-minimizing acquisition techniques, motion can be compensated on the post-processing level. The proposed approaches include co-registration by deformable or rigid transformations, segmentation and retrospective triggering (15,16).

A commonly used analysis of dynamic enhancement patterns is based upon a subjective

evaluation of the time-signal intensity curve, in which each curve is classified in accordance with the evaluation system shown in Fig. 8. Classification of signal intensity curves according to this scheme achieved very good diagnostic performance in differentiating malignant from benign lesions (17).

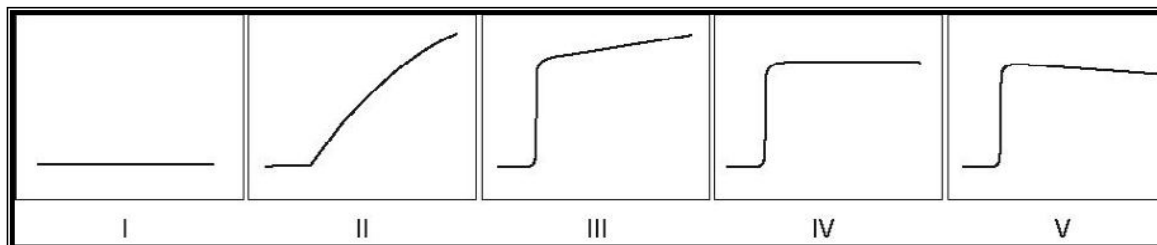


Fig. (2) The diagrams show the classification system for visual evaluation of the enhancement curves. I: no enhancement; II: slow sustained enhancement; III: rapid initial and sustained late enhancement; IV: rapid initial and stable late enhancement; V: rapid initial and decreasing late enhancement. **Quoted from Ingrid S. G. et al , (17).**

At sufficient temporal resolution, a normal SI-curve after Gd-chelate injection can be described by 3 phases. An early peak corresponds to the first pass of the contrast agent through the capillary bed. The second phase, characterized by a slow increase corresponds to the recirculation of the contrast agent and the glomerular–tubular transfer. The third phase is characterized by a slow decay of signal intensity and corresponds to the excretory function of the kidney (16,18).

A broad range of approaches have been taken to assess the properties of enhancement curves in various tumors. **Kaiser et al. (17)**, normalised the signal enhancement using the intensity of the lesion before contrast injection and defined malignant lesions as those showing a signal enhancement of at least 100% during the first minute. Other workers have identified the presence of very early enhancement in the tumor after the arrival of the arterial bolus as an indicator of malignancy (17).

The potential problems in the use of signal enhancement curves to study malignant vasculature are Firstly, signal intensity changes are non-specific and will vary according to a wide range of scanner parameters.

Because of the non-linear relationship between contrast concentration and signal intensity changes and the wide variation in baseline T1 values and signal intensity seen in the tissues being studied, attempts to calibrate or produce standard images which could be used in multiple sites have not been successful. Subjective enhancement curve analysis must therefore include some form of curve normalization to account for these variations which are principally seen as differences in the amplitude of the enhancement curve. Secondly, the enhancement curves will contain important information not only in terms of amplitude but also in terms of time of arrival and curve slope. The choice of normalization technique and of the most representative curve shaped parameter is difficult and has led to the development of many semi-quantitative or descriptive systems (17).

4. Diffusion Weighted imaging (DWI) of the kidney

Diffusion is a mass transport process arising in nature, which results in molecular or particle mixing without requiring bulk motion. Diffusion should not be confused with convection or dispersion-other transport mechanisms that require bulk motion to carry particles from one place to another (19).

Diffusion-weighted imaging (DWI) is a MR modality using strong bipolar gradients to create a

sensitivity of the signal to the thermally induced Brownian (or random walk) motion of water molecules and in vivo measurement of molecular diffusion (11).

Magnetic resonance provides a unique opportunity to quantify the diffusional characteristics of a wide range of specimens. Because diffusional processes are influenced by the geometrical structure of the environment, MR can be used to probe the structural environment non-invasively. This is particularly important in studies that involve biological samples in which the characteristic length of the boundaries influencing diffusion are typically so small that they cannot be resolved by conventional magnetic resonance imaging (MRI) techniques (19).

A typical nuclear magnetic resonance (NMR) scan starts with the excitation of the nuclei with a 90-degree radiofrequency pulse that tilts the magnetization vector into the plane whose normal is along the main magnetic field. The spins subsequently start to precess around the magnetic field – a phenomenon called Larmor precession. The angular frequency of this precession is given by $\omega = \gamma B$

Where B is the magnetic field that the spin is exposed to and γ is the gyromagnetic ratio – a constant specific to the nucleus under examination. In water, the hydrogen nucleus (i.e., the proton) has a gyromagnetic ratio value of approximately 2.68×10^8 rad/s/tesla (19).

The echo magnitude could be sensitized solely to the effects of random molecular spreading caused by diffusion in a way that permits a direct measurement. Because a spin's precession frequency is determined by the local magnetic field, if a “magnetic field gradient” is applied, spins that are at different locations experience different magnetic fields – hence they precess at different angular frequencies. After a certain time, the spins acquire different phase shifts depending on their location. Stronger gradients will lead to sharper phase changes across the specimen, yielding a higher sensitivity on diffusion. In most current clinical applications, a quantity called the “b-value”, which is proportional to the square of the gradient strength, is used to characterize the level of the induced sensitivity on diffusion (19).

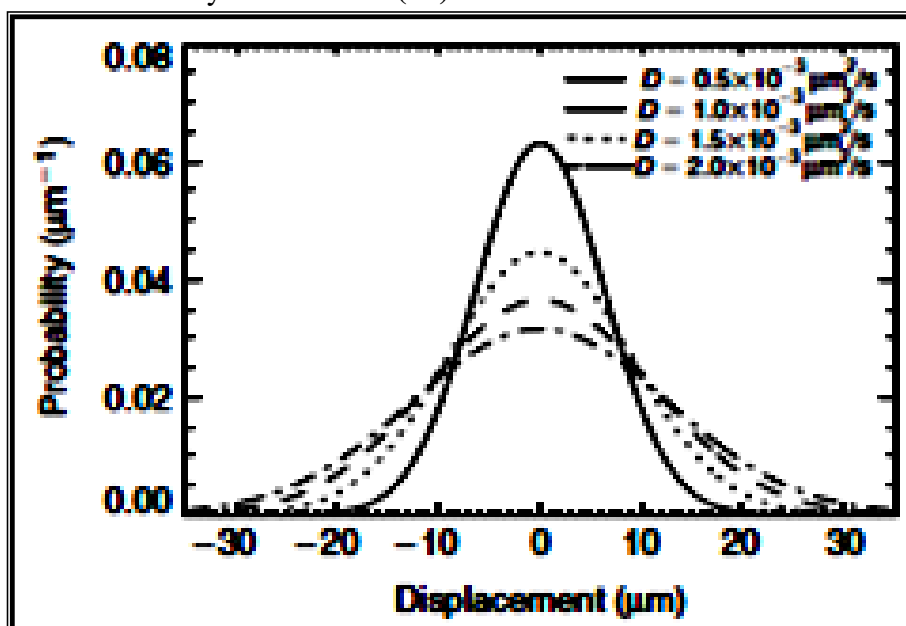


Fig:(3) The Gaussian displacement distribution plotted for various values of the diffusion coefficient when the diffusion time was taken to be 40 ms. Larger diffusion coefficients lead to broader displacement probabilities suggesting increased diffusional mobility. **Quoted from Peter J. et al,(19).**

The apparent diffusion coefficient (ADC) is a quantitative parameter calculated from DW images which is used as a measure of diffusion. Since the ADC is also dependent on capillary perfusion and water diffusion in the extra-vascular space, alteration of the ADC provides information concerning microstructural changes (11). The ADC of the kidneys is higher than the ADC of other abdominal organs, most likely due to the high-water content and the high blood supply of the kidneys and possible contributions of the flow in the tubular system(20,21).

In most studies, the cortical ADC was found to be higher than the medullary ADC, presumably because of the higher perfusion component. Blood and tubular flow as well as water content may change the ADC. Measurements of renal ADC have been detailed in various studies, showing that DWI is a feasible approach for the characterization of renal diseases and lesions (20,21).

Technique

DWI is commonly based on ultrafast single shot echo-planar imaging (EPI) sequences, which freeze bulk motions, making rapid acquisition mandatory, which limits the number of acquired slices as well as the spatial resolution. For calculation of the ADC at least two images are required, one with and one without application of a diffusion gradient. The diffusion weighting is expressed by the diffusion factor b . The ADC is measured in mm^2/s and represents the negative natural logarithm (\ln) of the ratio of signal intensities of the two images (S_0 is the signal at $b = 0$ and S_1 is the signal after application of the diffusion gradient): $\text{ADC} = (-1/b) [\ln (S_1/S_0)]$ (11). DWI does not only measure “pure” diffusion of water molecules, but also water motion in preformed structures, i.e. perfusion in the renal microvasculature or flow in the tubuli. The ADC depends on perfusion effects at lower b -values ($b < 200\text{s}/\text{mm}^2$) in their works on intravoxel incoherent motion (IVIM). These effects of pseudodiffusion can be excluded when high b -values ($b > 400\text{s}/\text{mm}^2$) are applied to obtain true diffusion measurements. Some authors have quantified the perfusion information of DWI using a bi-exponential fit of the ADC-curve and calculating the perfusion fraction to evaluate renal function (22,23). While there has been a first consensus on DWI-parameters for assessing tumors, there has been no consensus on the optimal parameters for DWI of the kidney, with maximal b -values ranging from 200 to $800\text{s}/\text{mm}^2$ (24,25). Studies performed in the brain suggest, that a higher number of b -values allow for a more accurate fit of the ADC-curve (26).

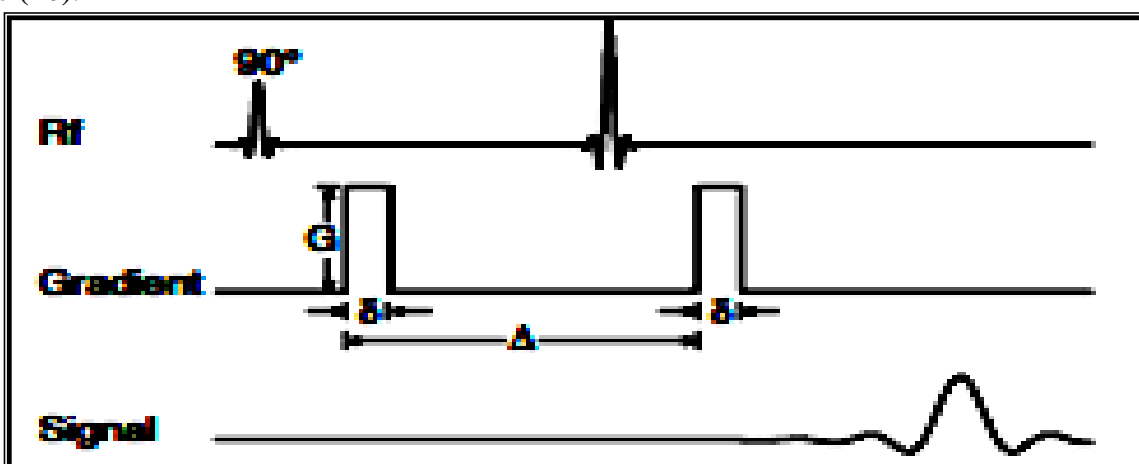


Fig:(4) A schematic of the pulsed field gradient spin-echo MR technique introduced by Stejskal and Tanner. The time between the application of the two gradient pulses, Δ may be anywhere between 10 ms and a few hundreds of milliseconds. The gradient pulse duration, γ can vary between a few milliseconds to Δ , where when $\gamma = \Delta$, the pulse sequence becomes the same as that in Figure 15. **Quoted from Peter J. et al,(19).**

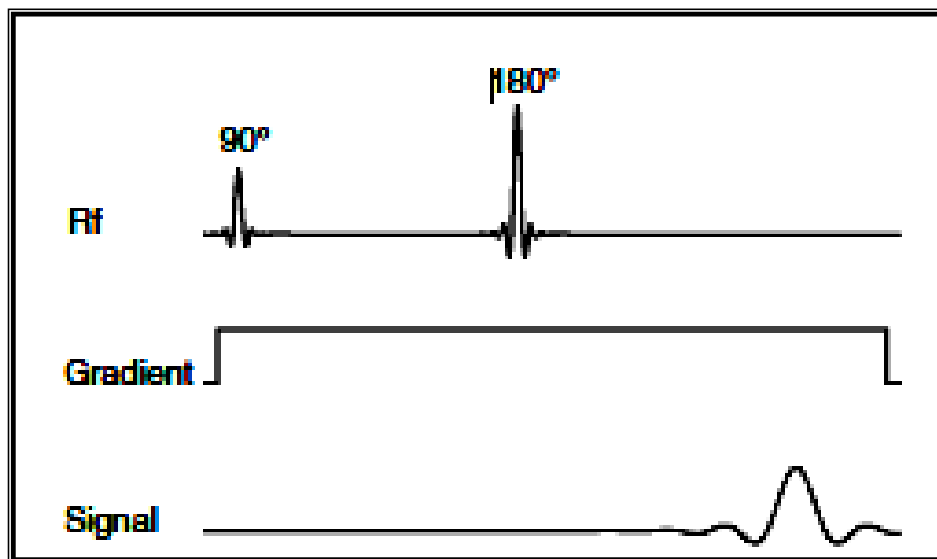


Fig:(5) A schematic of the spin-echo experiment in the presence of a constant field gradient discussed by Carr and Purcell. Diffusion taking place in the resulting inhomogeneous field gives rise to a decreased MR signal intensity. **Quoted from Peter J.et al, (19).**

Parallel imaging has already been successfully applied in abdominal DWI allowing increased resolution and acquisition speed with negligible alteration of diffusion values. Moreover, distortion artifacts caused by magnetic field inhomogeneities are reduced because of shorter readout times. Furthermore, as motion on a molecular level is measured, DWI is very sensitive to motion artifacts. Respiratory motion is one of the major obstacles to overcome. Another source of motion artifacts is the arterial pulsatility of the kidneys (11). Reproducibility of DWI of the kidney has been assessed with a free-breathing technique, showing promising results. The best image quality and reproducibility is gained when applying respiratory triggering (27,28).

For each DWI sequence, a pixel-by-pixel apparent diffusion coefficient (ADC) map was automatically calculated, with the gray value of the pixel linearly corresponding to the ADC value expressed in square millimeters per second (1).

The clinical application Dynamic contrast-enhanced MRI & Diffusion-weighted imaging (DWI) of the kidney

Kidney mass is the term used to describe a group of cells that have abnormally formed together on or in the kidney. Under normal circumstances, kidney cells grow and divide to form new cells that replace old or dead ones. However, sometimes cells form when the body doesn't need new ones, or old cells that should die, continue to live. A kidney mass of tissue commonly referred to as a kidney growth, kidney cyst, or kidney tumor, can develop from these extra cells (29).

Particularly when combined with T1- and T2-weighted MR imaging, the contrast-enhanced techniques are highly effective for characterization of renal masses owing to the ability to portray dynamic contrast enhancement. The ability to display venous structures with contrast-enhanced 3D FSPGR techniques helps staging of renal cell carcinoma (30). Gadolinium is widely used in contrast-enhanced dynamic imaging, usually using fast gradient echo (GRE) sequences with fat suppression. These protocols often include non-enhanced MRI sequences followed by post contrast imaging during arterial, venous, and nephrographic phases. More recently, the improved spatial and temporal resolution of current MR scanners allows the visualization of gadolinium contrast material within distinct time phases in distinct intra renal regions, such as the cortex, the

medulla, and the collecting system (31).

DWI is a technique which can delineate pathologic lesions with high tissue contrast against generally suppressed background signal. Findings on DWI can provide insight into the water composition of tumors and normal tissue. Pathologic processes such as inflammation and neoplasia tend to alter structural organization by destruction or regeneration of membranous elements or by a change in cellularity. Increased cellular density limits water diffusion in the interstitial space.

Thus, changes in permeability, osmolarity, and active transportation can occur concurrently. All of these changes can affect proton mobility and diffusivity, which can be observed with DWI (1).

5. Conflict of Interest: No conflict of interest.

6. References

1. **H. Chandarana and V. S. Lee. (2009):** Renal Functional MRI: Are We Ready for Clinical Application? *Am. J. Roentgenol.*, June 1; 192(6): 1550 – 1557.
2. **Ivan Pedrosa, Maryellen R. Sun, Matthew Spencer, et al. (2008):** MR Imaging of Renal Masses: Correlation with Findings at Surgery and Pathologic Analysis *RadioGraphics*; 28:985–1003.
3. **Cairns P.** Renal cell carcinoma. (2010) *Cancer biomarkers: section A of Disease markers*. 9 (1-6): 461-73.
4. **Cova M, Cavallaro M, Martingano P, and Ukmar M:** Magnetic resonance imaging of the kidney In Quiaia E (eds): *Radiological Imaging of the Kidney Springer, 2011*; 1st edition: 179-196.
5. **Pallwein-Prettner L, Flöry D, Rotter C et al.** Assessment and characterization of common renal masses with CT and MRI. *Insights Imaging*, 2011; 2(5): 543–556.
6. **Srinivasa R. Prasad, Peter A. Humphrey, Christine O, et al., (2005):** Neoplasms of the Renal Medulla: Radiologic-Pathologic Correlation. *RadioGraphics* 2005; 25:369–380.
7. **Bloom TL, Gray Sears CL, Williams TR, Linfesty RL, Amling CL.** Multilocular cystic renal cell carcinoma with osseous metaplasia in a 25-year-old woman. *Urology* 2003; 61:462.
8. **Eble JN, Sauter G, Epstein IJ, Sesterhenn IA.** WHO Classification of Tumours of the Urinary System and Male Genital Organ. Lyon, France: International Agency for Research on Cancer (IARC) Press, 2004.
9. **Brant W.E. (2007):** genitor urinary tract IN Brant W.E. and Helms C.A. (Eds): *Fundamentals of Diagnostic Radiology*, 3rd edition; chapter 33: P 174-184.
10. **Grenier N, Basseau F, Ries M, Tyndal B, Jones R and Moonen C. (2003):** Functional MRI of the kidney. *Abdominal Imaging*; 28(2):164–75.

11. **Low RN, Sebrechts CP, Barone RM, et al., (2009).** Diffusion-weighted MRI of peritoneal tumors: comparison with conventional MRI and surgical and histopathologic findings-a feasibility study. *AJR Am J Roentgenol*; 193:461-70.
12. **Sourbron SP, Michaely HJ, Reiser MF, and Schoenberg SO.(2008):** MRI-measurement of Perfusion and glomerular filtration in the human kidney with a separable compartment model. *Invest Radiol*; ch 43: p 40–8.
13. **Bokacheva L, Rusinek H, Zhang JL, Chen Q, and Lee VS.(2009):** Estimates of glomerular filtration rate from MR renography and tracer kinetic models. *J MagnReson Imaging*; 29(2):371–82.
14. **Hackstein N, Kooijman H, Tomaselli S and Rau WS.(2005):** Glomerular filtration rate measured using the Patlak plot technique and contrast-enhanced dynamic MRI with different amounts of gadolinium–DTPA. *J MagnReson Imaging*; 22; p: 406–14.
15. **Attenberger U, Sourbron S, Michaely H, et al., (2008):** Retrospective respiratory triggering for 2D abdominal perfusion MRI. *Proc Intl Soc Mag Reson Med*; 16:462.
16. **Michaely HJ, Schoenberg SO, Oesingmann N, et al., (2006):** Renal artery stenosis: functional assessment with dynamic MR perfusion measurements feasibility study. *Radiology*; 238(2):586–96.
17. **Ingrid S. G., Kjell I. G., Gunnar N., Steinar L.,Mari H. B., and Alan J. (2005):** Dynamic Contrast-Enhanced Magnetic Resonance Imaging in Oncology : MEDICAL RADIOLOGY Diagnostic Imaging Principles of Dynamic Contrast-Enhanced MRI .An Introduction to Dynamic Contrast-Enhanced MRI in Oncology p3-22.
18. **Dujardin M, Sourbron S, Luybaert R, Verbeelen D, Stadnik T. (2005):** Quantification of renal perfusion and function on a voxel-by-voxel basis: a feasibility study.*MagnReson Med*;54(4):841–9.
19. **Peter J. Basser and EvrenÖzarslan. (2009):** Diffusion MRI from quantitative measurement to in-vivo neuroanatomy: chapter 1, Introduction to Diffusion MR, Pages3-11.
20. **Laissy JP, Idee JM, Fernandez P, Floquet M, Vrtovsnik F and Schouman-Claeys E. (2006):** Magnetic resonance imaging in acute and chronic kidney diseases: present status. *Nephron Clin Pract*; 103 (2): c50.
21. **Thoeny HC, De Keyzer F, Oyen RH and Peeters RR. (2005):** Diffusion-weighted MR imaging of kidneys in healthy volunteers and patients with parenchymal diseases: initial experience. *Radiology*; 235(3):911–7.
22. **Blondin D, Lanzman RS, Mathys C, et al., (2009):** Functional MRI of transplanted kidneys

- using diffusion-weighted imaging. *Rofo*; 181(12):1162–7.
23. **Padhani AR, Liu G, Koh DM, et al., (2009):** Diffusion-weighted magnetic resonance imaging as a cancer biomarker: consensus and recommendations. *Neoplasia*; 11(2):102–25.
24. **Lee VS, Rusinek H, Bokacheva L, et al., (2007):** Renal function measurements from MR renography and a simplified multicompartamental model. *Am J Physiol Renal Physiol*; 292(5):F1548–59.
25. **Namimoto T, Yamashita Y, Mitsuzaki K, Nakayama Y, Tang Y, Takahashi M. (1999):** Measurement of the apparent diffusion coefficient in diffuse renal disease by diffusion-weighted echo-planar MR imaging. *J Magn Reson Imaging*; 9; p:832–7.
26. Potential and Limitations of Diffusion-Weighted Magnetic Resonance Imaging in Kidney, Prostate, and Bladder Cancer Including Pelvic Lymph Node Staging: A Critical Analysis of the Literature. *European. Volume, February, Pages 326–340.*
27. **Notohamiprodjo M, Dietrich O, Horger W, et al., (2010):** Diffusion tensor imaging (DTI) of the kidney at 3 Tesla feasibility, protocol evaluation and comparison to 1.5 Tesla. *Invest Radiol*; 45(5):245–54.
28. **Kwee TC, Takahara T, Koh DM, Nieuwelstein RA and Luijten PR.(2008):** Comparison and reproducibility of ADC measurements in breathhold, respiratory triggered and free-breathing diffusion-weighted MR imaging of the liver. *J Magn. Reson. Imaging*; 28(5):1141–8.
29. **Higgins JC and Fitzgerald JM. (2001):** Evaluation of incidental renal and adrenal masses. *Am Fam Physician*. Jan 15; 63(2):288-94, 299.
30. **Christine Menias, Srinivasa R Prasad, Ankitkumar H. et al., (2008):** Neoplastic and Nonneoplastic Proliferative Disorders of the Perirenal Space: Cross-sectional Imaging Findings Venkateswar R. Surabhi, *RadioGraphics*; 28:1005–1017.
31. **Yuelang Z, Xingwang S, Guangnan Q, Yongqian Q and Chenxia L.(2008):** Value of Apparent Diffusion Coefficient(ADC) of Diffusion Weighted Magnetic Resonance Imaging in Common Renal Disease Diagnosis. *Journal of Nanjing Medical University*, Volume 22, Issue 6, November, Pages 362-365 ; Available online 14 July 2009.